Published in final edited form as:
NMR Biomed. 2014 February ; 27(2): 163–174. doi:10.1002/nbm.3048.

Assessment of ischemic penumbra in human hyperacute stroke patients using amide proton transfer (APT) Chemical Exchange Saturation Transfer (CEST) MRI

Anna Tietze[1,2,*], **Jakob Blicher**[2,3], **Irene Klærke Mikkelsen**[2], **Leif Østergaard**[1,2], **Megan K. Strother**[4], **Seth A. Smith**[4,7], and **Manus J. Donahue**[4,5,6,7]

[1]Department of Neuroradiology, Aarhus University Hospital, Aarhus, Denmark

[2]Center of Functionally Integrative Neuroscience, Aarhus University Hospital, Aarhus, Denmark

[3]Hammel Neurorehabilitation and Research Center, Aarhus University Hospital, Hammel, Denmark

[4]Department of Radiology, Vanderbilt University School of Medicine, Nashville, TN

[5]Department of Psychiatry, Vanderbilt University School of Medicine, Nashville, TN

[6]Department of Neurology, Vanderbilt University School of Medicine, Nashville, TN

[7]Physics and Astronomy, Vanderbilt University School of Medicine, Nashville, TN

Abstract

Chemical exchange saturation transfer (CEST)-derived pH-weighted Amide Proton Transfer (APT) MRI has shown promise in animal studies for predicting infarction risk in ischemic tissue. Here, APT MRI was translated to acute human stroke patients (1–24 hrs post-symptom-onset) and assessments between APT contrast, perfusion, diffusion, disability, and final infarct volume (23–92 days post-stroke) are reported. Healthy volunteers (n=5) and patients (n=10) with acute onset of symptoms (0–4h: n=7; uncertain onset <24h: n=3) were scanned with diffusion- and perfusion-weighted MRI, FLuid Attenuated Inversion Recovery (FLAIR) and CEST. Traditional asymmetry as well as a Lorentzian-based APT index were calculated in the infarct core, at-risk tissue (time-to-peak, TTP, lengthening), and the final infarct volume. On average (mean±s.d.), control white matter APT values (asymmetry: 0.019±0.005; Lorentzian: 0.045±0.006) were not significantly different (P>0.05) than APT values in normal-appearing-white-matter (NAWM) of patients (asymmetry: 0.022±0.003; Lorentzian: 0.048±0.003), however ischemic regions in patients had reduced (P=0.03) APT effects compared to NAWM. Representative cases are presented whereby the APT contrast is compared quantitatively to contrast from other imaging modalities. Findings vary between patients; in some patients a trend for a reduction of the APT signal in the final infarct region compared to at-risk tissue was observed, consistent with tissue acidosis. However, in other patients no relationship was observed in the infarct core and final infarct volume. Larger

[*]Corresponding Author: Anna Tietze, tel.: +45 78469953, fax: +45 78463360, anntie@rm.dk, Dept. of Neuroradiology, Nørrebrogade, bldg. 10, 8000 Aarhus C, Denmark.

Conflict of Interest Disclosure
The authors do not have any conflict of interest to disclose with regards to the material in this manuscript.

clinical studies in combination with focused efforts on sequence development at clinically available field strengths (e.g., 3.0T) are necessary to fully understand the potential of APT imaging for guiding hyperacute management of patients.

Keywords

CEST; stroke; pH; penumbra; blood flow; amide proton transfer

Introduction

Acute stroke therapy is contingent on the identification of tissue at risk of infarction. The target of stroke therapy is thus the “ischemic penumbra”: ischemic tissue that may remain viable and whose function can be restored by recanalization therapy. Intravenous or intra-arterial administration of recombinant tissue plasminogen activator (tPA) and endovascular procedures (EP) such as mechanical thrombectomy have been shown to increase reperfusion rates and to reduce final infarct size when administered within the first 4.5 hours of symptom onset (1–3). Importantly, recanalization therapy carries the risk of hemorrhagic events, which occur in approximately 6 % of patients treated with EP or tPA (4). Therefore, fast imaging tools that accurately identify both the ischemic penumbra and the ischemic core of irreversibly damaged tissue are of great importance for optimal individualized therapy.

Prior to treatment, the infarct core and penumbra are commonly estimated by perfusion computed tomography (CT) or perfusion- and diffusion-weighted MRI (PWI and DWI). Hyperintense regions on DWI (or hypointense on apparent diffusion coefficient, ADC, maps) are typically thought to represent the ischemic core, yet in some patients subregions of the DWI lesion may not progress to infarction (5,6). Hypoperfused regions on PWI maps typically include core, penumbra, and areas of benign oligemia in which the tissue survives spontaneously without the need of recanalization (7–10) and it is currently not possible to distinguish these regions in many patients using existing imaging procedures. It is therefore desirable to pursue new imaging approaches that may be capable of defining the penumbra more precisely (11).

This could be addressed by detecting the metabolic characteristics of the ischemic penumbra. The penumbra may exhibit increased oxygen extraction and anaerobic glycolysis in the effort to maintain trans-membrane ion gradients. Anaerobic metabolism leads to tissue acidosis and thus acidosis may provide a sensitive indicator of impairment. It has been demonstrated that the signal intensities of amide protons exchanging with water are influenced by pH through principles of exchange-related saturation, and that this effect can be assessed using proton NMR spectroscopy (12). More recently, Amide Proton Transfer (APT) Chemical Exchange Saturation Transfer (CEST) MRI has been identified as a promising pH-sensitive MRI method (13,14). Whole-brain APT MRI can be obtained using standard equipment available at most hospitals and using commonplace imaging readouts that have already been optimized for structural and functional MRI. Chemical information is obtained through saturation transfer of magnetization between amide protons (primarily on the peptide backbone; *in vivo* concentration ~ 70–100 mM) and the imaged water protons

(concentration ~ 110 M). In APT, the labile protons originate from amide groups resonating at 8.3 ppm in the proton spectrum (+3.5 ppm from water) (13). Importantly, over a physiological pH (pH > 5), the exchange rate is base-catalyzed and therefore the APT effect-size on the water signal reduces with decreasing pH, or tissue acidosis. As anaerobic metabolism during ischemia leads to considerable tissue acidosis, APT permits insight into the energy status of ischemic parenchyma by indirect pH imaging. Sun et al. have demonstrated potential for this method by monitoring the evolution of pH changes following middle cerebral artery occlusion in anaesthetized rats at 4.7 T (15,16). However, owing to difficulties in adding novel MRI methods to hyperacute stroke protocols, it has not yet been possible to evaluate the potential of APT for increasing specificity to the ischemic penumbra in human stroke patients. Furthermore, the molecular sequelae of stroke are highly sensitive to the location and extent of ischemia, and thus involve a cascade of events that broadly involve excitotoxicity, oxidative stress, inflammation, and apoptosis (17–19). *Importantly, these events may elicit complex changes in APT contrast, as well as tissue T2 or T1*.

Here we present the application of pH-weighted APT MRI in hyperacute stroke patients (1–4.5 h post-symptom onset), in whom a more precise delineation of the penumbra could have an immediate impact on treatment decisions. Patients are scanned acutely using standard clinically available MRI equipment and invited for a follow-up at approximately 30 days to investigate the extent to which APT MRI predicts final infarction volume. We demonstrate that APT MRI is feasible in the acute setting on a busy neuroradiological unit and that pH-weighted tissue changes are detectable in infarct core and penumbra. However, it is also observed that APT contrast in humans at clinically available field strengths is more difficult to interpret than at high field strength in anaesthetized animals. Therefore, more robust, quantitative modeling approaches must be developed before this method is to be applied in a large-scale clinical trial (20–23). We discuss unexpected findings and relevant obstacles that should be addressed prior to large-scale clinical trials. These results have been partially published in abstract form (24).

Experimental

Subjects

This study was approved by the Danish Committee on Health Research Ethics (jr.-no. 1-10-72-118-12) and the Danish Data Protection Agency (jr.-no. 1-16-02-42-12). A total of ten patients (69 +/− 9 yrs) with onset of acute stroke symptoms from the anterior or posterior circulation were included in this study. Seven patients were imaged < 4 hours after onset of symptoms (average 2 hours, 7 min +/− 1 hour, 7 min). Three had a history with more uncertain time of onset (between 1 hour and 24 hours). In order not to delay stroke treatment, only patients awaiting mechanical thrombectomy, or patients found unsuited for thrombolysis by the treating neurologist (not involved in the study), were included. In three patients thrombolysis was given, but the decision was made after the MRI. Eight of the ten patients completed the follow-up MRI. As a control we performed APT imaging in five healthy subjects (38 +/− 7 yrs) on the same scanner using an identical CEST APT protocol as outlined below. Data were acquired in the control volunteers to ensure that the relatively fast and low-power CEST protocol provided contrast that was consistent with existing

models, and to understand how APT effects using this method varied between different healthy tissue types.

MRI protocol

MRI was performed on a 3T Philips® Achieva 3TX system in the acute setting. The acute imaging protocol included the following sequences: DWI (TR/TE=3596/98 ms; spatial resolution: 1.2x1.2x4 mm^2; 26 slices; 3 directions; max. b-value: 1000 s/mm^2), T2 FLAIR (TR/TE=11000/125 ms and TI=1800 ms; spatial resolution: 0.9x1.1x4 mm^2; 26 slices), CEST APT imaging (3D gradient echo with a single shot TFE readout (TFE factor = 36), B_1 = 0.5 μT, block pulse, 200ms duration, Δω spanned +5 to −5 ppm in 33 steps (0.31 ppm increments) plus 3 acquisitions far off resonance (80 kHz) for normalization; TR/TE/flip angle = 4.6 ms/2.4 ms/15°; nominal spatial resolution = 2.5x2.5x5 mm^3; slices = 16, SENSE = 2.5, binomial water excitation), and dynamic susceptibility-contrast imaging with TR/TE=1500/30 ms; spatial resolution = 1.9x1.9x4 mm^2; slices = 28; dynamics = 50 with a dynamic scan time of 1.5s; 0.1mmol/kg gadobutrol; 5 ml/s). The entire acute protocol had a duration of 10 min 52s, and the CEST sequence specifically had a duration of 3min 20s.

The final infarct size was assessed by follow-up T2 FLAIR imaging (TR/TE 8000/100ms and TI 2370ms; 0.9x1.1x4 mm^2; 42 slices). The follow-up scan was performed on a 3T Siemens® MAGNETOM Trio™. As FLAIR is a standard structural sequence, which provides very similar contrast between vendors, and the TR/TI was optimized on each scanner, different MRI systems for the acute and follow-up scan were considered to be acceptable. The follow-up scan only included FLAIR imaging for final infarct classification.

Image and data analysis

A summary of the data analysis procedure is illustrated in Fig. 1. All data were processed using Matlab (Mathworks, Natick, MA, USA). Dynamic susceptibility-contrast MRI data were pre-processed as described previously, and time-to-peak (TTP) maps were calculated (25,26). Masks were generated using a modified Gaussian mixture model and tools available in SPM (27). These masks were used to characterize tissue (i) in the ischemic “core” with high risk of infarction (hypointense on acute ADC), (ii) in the “at-risk” region defined by prolonged relative TTP, (iii) in the “final infarct” volume as defined by hyperintensity on the follow-up FLAIR scan, and (iv) in normal-appearing-white-matter (NAWM) taken as white matter contralateral to the ischemic hemisphere. Calculated maps were then confirmed and modified if necessary by a neuroradiologist (AT, neuroradiologist with four years experience in PWI).

Prior to voxel-wise analysis, each dynamic of the CEST spectra was corrected for motion using a 3D 6 degree-of-freedom rigid body transformation whereby each dynamic was registered to the initial volume. For each voxel, the CEST z-spectrum was calculated as: $S(\Delta\omega)/S_0$ where $S(\Delta\omega)$ is the signal obtained at offset frequency = Δω, and S_0 is the acquisition far from the water resonance. Due to coexisting MT effects, in some cases, CEST data obtained at $\Delta\omega = \pm 5$ppm did not return to a maximal value, $S(\Delta\omega)/S_0 = 1$. To minimize the impact of the global MT effect, noise arising from motion, and establish an upper bound for fitting the CEST z-spectrum to a Lorentzian lineshape, we: (i) renormalized

the CEST z-spectrum for each voxel by the average signal intensity obtained at $\Delta\omega = \pm$ 5ppm (similarly this could be addressed by adding a baseline term to the Lorentzian analysis as in Jones et al (28), and (ii) padded the z-spectrum by forcing the z-spectrum outside $\Delta\omega = \pm 5$ to be unity. It is important to consider that the MT effect on the observed CEST spectrum can span hundreds of ppm and thus, the renormalization procedure we adopted mitigates the impact of MT confounds on the APT resonance. To correct for B_0 inhomogeneity, CEST spectra were fit to a single Lorentzian (29) and the offset of the minimum CEST signal intensity was set to $\Delta\omega = 0$ ppm. To characterize the APT effect, the difference between the Lorentzian fit and the normalized, B_0-corrected z-spectrum was calculated near the APT resonance ($\Delta\omega = 3.5+/-0.3$ ppm) for every voxel and the resulting maps referred to as 'APT Lorentzian'. Acute and follow-up data were co-registered to acute FLAIR. Alternatively, the CEST-derived APT asymmetry was recorded, which was calculated here as the ratio of the mean z-spectrum values at −3.2, −3.5 and −3.8 ppm to those at +3.2, +3.5 and +3.8 ppm. Due to the NOE and aliphatic resonances opposite the APT resonance ($\Delta\omega = 3.5$ ppm) we chose as our primary measure the APT Lorentzian approach. We further postulate that since the NOE and aliphatic changes that may occur in acute stroke are not well understood that the interpretation of the APT effect when calculating an asymmetry spectrum could be unnecessarily complicated by unknown macromolecular changes.

A Wilcoxon Rank Sum test was applied to evaluate differences between regions.

Simulation

It is important to note that the CEST MRI protocol that was selected for this study uses a moderate length, yet low amplitude RF saturation pulse to provide CEST contrast (c.f. MRI protocol). There are three advantages of the lower power pulse: (i) minimization of the global MT contamination and direct water saturation on the CEST z-spectrum, (ii) the B1 power is on the order of the expected exchange rate of amide protons (~30 Hz), and (iii) the method can be performed rapidly within SAR limitations. The last point is critical as this protocol was designed to study patients in the most acute phase of stroke where time constraints were substantial. Therefore, to provide evidence for the CEST contrast observed in the patients, we simulated the expected APT effects using the Bloch equations incorporating chemical exchange using a three pool model (30) which takes into account the amide proton pool, the asymmetric MT effect, and the direct water saturation. To perform the simulations, we input the experimental scan parameters used in our 3.0T protocol (c.f. methods). Z-spectra were simulated using amide proton $k_{ex} = 30$ Hz (31), 100 mM concentration (centered at $\Delta\omega = 3.5$ppm) with a T1 = 400 ms (32,33) and T2 = 40 ms, for the MT component: $k_{ex} = 20$ Hz, 10M concentration (centered at $\Delta\omega = -2.5$ppm (34)), with a T1 = 1s, T2 = 10 μs, and for tissue water (direct saturation), 100 M concentration (centered at $\Delta\omega = 0$ppm), $T_1 = 1$s, and T2 = 80 ms (35). It should be pointed out that a range of amide proton exchange rates have been simulated and calculated from CEST spectra. However, due to the low pulse power of the CEST saturation chosen for *in vivo* imaging, the lower exchange rate species will be more efficiently saturated and thus we simulated the impact of a change of pH on an exchange rate that is on the order of the B_1 saturation power (36). We then simulated the impact of decreased pH assuming a decrease in the pH from 7.1 to 6.5, which results in a decrease in k_{ex} from 30 Hz to 7 Hz (31). Additionally, it is possible that

an increase in the amide proton concentration can offset the decrease in k_{ex} arising from only pH effects. This is particularly challenging to model as *in vivo* the exchange rate may be evolving simultaneously with changes in amide proton concentration. However, to model the change in concentration without a pH-driven alteration in the exchange rate, we hypothesized that there may be as much as a 30% increase in the amide proton concentration (though this value is speculative) in acute stroke. Thus, we performed a simulation at pH = 7.1, amide proton concentration = 130 mM and k_{ex} = 30 Hz. It should be noted that the impact of pH and concentration changes on the CEST observation, while significantly different in their biophysical properties, ultimately can be coalesced into one simulation difference: a change in the exchange rate. Thus it is not possible with only a 3-pool model to separate a pH-driven decrease in k_{ex} and change in concentrations independently. Note that in our simulations we chose to keep the water concentration and relaxation properties constant, which may not be a complete description of the phenomena that exist *in vivo* for acute stroke. Thus, concentration changes in the presence or absence of exchange rate alterations may confound abilities to characterize the relative contributions of each pathological substrate.

Results

Healthy volunteers

The APT asymmetry values (mean±s.d.) in healthy control volunteers were: 0.016±0.006 (gray matter), 0.019±0.005 (white matter), and 0.017±0.008 (CSF). The APT Lorentzian values were: 0.039±0.008 (gray matter), 0.045±0.006 (white matter), and 0.033±0.008 (CSF). The coefficient of variation using the asymmetry approach was found to be: 0.36 (gray matter), 0.23 (white matter), and 0.43 (CSF), versus for the Lorentzian approach: 0.21 (gray matter), 0.12 (white matter), and 0.23 (CSF). Therefore, in control volunteers, the extent of variation of the mean APT measurement was found to be approximately 83% lower when using the Lorentizan approach versus the asymmetry approach, the latter of which is known to be more sensitive to contributions from the Nuclear Overhauser Effect and spectral asymmetric magnetization transfer effects (37). Fig. 2 shows graphically the results from the control volunteer analysis in different tissue types and for the different analysis approaches.

Simulation

Fig. 3 shows the expected z-spectra and the Lorentzian fit around the amide proton resonance ($\Delta\omega$ = 3.5 ppm). It can be seen that these parameters reveal an expected, small APT effect of 0.016 in white matter, which agrees reasonably well with the experimental data (Fig. 2). Assuming a pH decrease from 7.1 to 6.5 (k_{ex} from 30 Hz to 7 Hz), a reduced APT effect is predicted indicating the suspected reduction in contrast when tissue is acidotic. Finally, assuming a 30% larger amide proton concentration (independent of exchange rate increase), Fig. 3 shows the potential increase in the APT effect at $\Delta\omega$ = 3.5 ppm resulting in an APT effect ~ 0.017.

Stroke patients

Table 1 summarizes the patient information. Six patients had anterior circulation infarcts, two patients posterior circulation infarction, and two patients had two separate infarcts involving both the anterior and posterior circulation as defined by acute diffusion restriction. A total of 14 acute infarcts were detected. Three patients were diagnosed with large middle cerebral artery infarctions; the remaining patients had strokes involving minor vascular territories. Mean volume of the ischemic core was 11.1 ± 17.4 mL and the mean volume of the region demonstrating TTP lengthening was 78.7 ± 88.9 mL. In patients with penumbra, the mean volume of the penumbra (DWI/PWI mismatch) was found to be 86.8 ± 76.9 mL.

Table 2 summarizes all imaging findings. The number of subjects in each category varies depending on whether the specified region was observed: All patients (n = 10) exhibited an ischemic core, six exhibited a penumbra, two subjects could not be scanned at follow-up due to death/morbidity; and one did not show any final infarct volume. As expected, ADC was not different ($P = 0.25$) between the region with TTP lengthening and the penumbra tissue, however was significantly lower ($P < 0.001$) in both the ischemic core and tissue progressing to infarction compared to penumbra. Only a small trend for an effect ($P = 0.10$) was found between the TTP in the penumbra and in the final infarct volume. There were no significant regional group-level differences in the acute T2 FLAIR data, however there was a trend for an increase in acute T2 FLAIR signal intensity, indicative of T2 lengthening, in the region progressing to final infarct relative to the region with TTP-lengthening ($P = 0.08$). NAWM APT effect size was not significantly different from that in control volunteers, and was also significantly higher than in all of the ischemic regions considered ($P=0.03$ in all ischemic regions). A trend for a mean reduction in APT was found between the region of TTP-lengthening and final infarct volume ($P = 0.10$). The extent of the penumbra, stroke location, time post-symptom onset, treatment, and outcomes all varied considerably between patients. Therefore, it is most useful to consider the patients individually to understand the potential of CEST for assisting in penumbra demarcation.

Fig. 4 shows the tissue progressing to infarction in an example patient (Patient 4; Table 1), along with the hyperacute APT maps calculated from the asymmetry and Lorentzian methods. The Lorentzian method provides contrast more visually consistent with the pathology than does the asymmetry map, which can be attributed to substantial un-corrected intra-scan motion that varied between offsets or NOE/aliphatic changes that are not included in the APT Lorentzian map. *However, the contrast is only partially consistent with the hypothesis that APT effects should be reduced in tissue progressing to infarction, and also contains clear contrast in chronic infarcts.* The z-spectrum for this patient is shown separately in Fig. 5.

As can be seen in Fig. 6, in 8/10 patients, the Lorentzian APT analysis was tightly correlated with the asymmetry analysis ($R=0.72$; $P=0.02$). However, in two patients with very small ischemic regions, the APT asymmetry analysis provided negative values that were more than two standard deviations beyond the group mean (white circles; representative TTP maps shown with arrows pointing to TTP lengthened regions). Fig. 7. summarizes the group results for both analysis approaches.

Finally, Fig. 8 shows an additional example patient (Patient 1; Table 1) who presented with a large ischemic penumbra but less noticeable asymmetry relative to the patient shown in Fig. 4, and also who has a much smaller region of final infarction. Multiple considerations that may influence the APT contrast in this and other patients are discussed in the following section.

Discussion

This is one of the first studies applying APT imaging in acute stroke patients presenting within the thrombolysis treatment window. The major findings of this study are (i) APT contrast is reduced, on average (Fig. 7), in ischemic regions of patient volunteers relative to the normal-appearing white-matter of both healthy and patient volunteers, and (ii) even in a small subgroup of patients, APT contrast shows potential for correctly predicting final infarct volume in patients with acute ischemic stroke, *however contrast is complex with multiple experimental and physiological considerations*.

CEST in acute stroke

APT imaging in stroke patients has been investigated in one previous study (38), however, imaging was first performed 1 – 7 days after onset of symptoms. Interpretation of APT changes in these subacute phases is not straightforward as several factors can influence the signal. For example, persisting energy failure due to vessel occlusion, proteolysis and inflammation are likely to increase the amount of mobile amides leading to a larger APT effect opposing the change induced by lower pH. It should be noted however that this effect (change in amide proton concentration) was assessed in animals using exchange spectroscopy during the initial ischemic period postmortem and no changes could be found (31). Moreover, washout of lactate as a consequence of partial reperfusion, buffering processes or even small temperature variations can influence the signal. It has even been shown that a shift from acidosis to alkalosis in subacute cerebral ischemia takes place, which makes consideration of lesion age even more important when evaluating APT changes (39). Importantly, patients presented here were scanned in the hyperacute setting within the treatment window. The patients presenting with a penumbra had non-significant signal lengthening on acute T2 FLAIR, confirming the assumption of largely unchanged water content. Interestingly, the ischemic core (defined from the ADC hypointensity) did not have a significantly different APT value relative to the penumbra. While a lower APT effect is consistent with tissue acidosis, it is surprising that an identical APT effect may be found in the ischemic core. Jokivarsi et al. made a similar observation of APT pseudo-normalization in a middle cerebral artery occlusion rat model in spite of delayed lactate clearance (40). They suggested early buffering processes or temperature alterations in the infarct core might explain this unexpected finding. Another possibility for this finding is that small regional changes in T2 alter the lineshape of the direct saturation compoenent of the CEST z-spectrum, which may lead to an apparent change in the magnitude of the APT effect (yet are derived from T2 lineshape broadening and/or narrowing), especially when using a single Lorentzian to characterize the CEST z-spectra. Similarly, in regions of prior infarct, tissue atrophy, or even voxels that partial volume substantially with CSF, the longer T1 of the fluid in the voxel will also change the direct saturation lineshape (41) and thus may result in a

significant change in the observed CEST z-spectrum (less efficient saturation, changes in the direct saturation component, a constant offset of the z-spectrum). Therefore, one known drawback of fitting the CEST z-spectra in voxels that contain different tissues, or species of different relaxation times, exchange rates and concentrations is that a fit of the CEST spectrum to a single Lorentzian cannot capture the complexity of the interactions in a sub-voxel manner. Therefore, more sophisticated models could be pursued, however it is unclear whether the data quality available in fast (3–4 min), moderate-field (e.g., 3.0T) sequences is sufficient for such investigations at present.

It is also unlikely that this effect is due to gliosis. Gliotic scar tissue consists of reactive astrocytes, oligodendrocyte progenitor cells, microglia, and possibly peripheral inflammatory cells. The final scar tissue contains connective tissue elements that are believed to occur in subacute or chronic phases and therefore this is unlikely to be a substantial confound in acute stroke. In more chronic patients, this effect would alter T1 and could lead to artifactual APT effects.

The two patients shown here summarize the overall motivation for this work. For instance, both patients (Fig. 4 and Fig. 8) presented with large ischemic penumbras, yet the final infarct volume is most substantial in the patient in Fig. 4. Both patients underwent similar treatment. Imaging methods that can predict this result would be of great interest for guiding aggressive therapy decisions. Here, the patient in Fig. 4 demonstrated clear asymmetric APT contrast that was consistent with tissue acidosis. This APT contrast was in both the region of acute ischemia as well as in a region of prior infarct; therefore, similar to other imaging modalities it will be important to consider contrast in acutely ischemic regions preferentially for making informed treatment decisions. The patient in Fig. 8 exhibited no clear asymmetry in acute APT contrast and also had a much smaller region of final infarction. However, the APT maps are also subject to many complications, including motion (which can be clearly seen on the FLAIR image of this patient), as well as partial volume effects between tissues with different T1 and T2, and low SNR at 3T. As the values in this patient were highly variable across the slice, it cannot be concluded that poor data quality, rather than a lack of tissue acidosis, is the underlying source of the contrast. Avenues for improving APT contrast are discussed below.

Technical considerations

We were in most cases able to visualize lateralizing contrast on APT maps. However, the lesions appear to need a certain size before they become discernible on APT-weighted images, and infarcts in the posterior fossa are particularly prone to be obscured by artifacts. Similarly, as shown in Fig. 6, quantitative asymmetry analysis in very small lesions is difficult owing to very few voxels available for analysis, and propagation of error that exists by comparing data points acquired at different times (e.g., +/− 3.5 ppm). Others have earlier observed CSF-related artifacts, when lesions are in the vicinity of the ventricles, a fact that can lead to diagnostic misapprehension (38). Patient movement during image acquisition, a common problem in the acute setting of stroke imaging, can compromise diagnostic quality considerably. A CEST sequence for acute stroke imaging needs to be very fast, and

therefore only a limited number of offset measurements can be performed leaving the technique extremely sensitive to noise and motion.

Importantly, much of the CEST development focuses on mechanistic studies of the contrast mechanism in phantoms or anaesthetized animals, frequently at very high field strength (4.7–7.0 T). While these parameters are better suited for understanding CEST contrast, it remains unclear whether such methods can be translated to commonly available clinical systems at 3.0T and below, where SNR and exchange rates are much reduced. This study does provide some support for transitioning CEST to acute stroke imaging at commonly available field strengths, however additional development work is required for optimizing fast (< 5 min), low-power motion-desensitized acquisitions for this clinical population.

To this end, the sequence parameters were chosen here to provide a rapid estimate of the APT effect in patients with acute stroke. It should be noted that the pulse power used in this study is significantly lower than what is conventionally used for CEST MRI. The benefit to a reduced power can be summarized as follows: (i) an RF irradiation power on the order of the expected exchange rates for amide protons (~30 Hz) is relatively insensitive to MT and direct water saturation, which alter the baseline, NOE, aliphatic resonances in tissues undergoing transient changes as in stroke; (ii) potential T1 and T2 confounds are reduced by using a pulse length that is significantly less than T1 but greater than T2; (iii) the sensitivity to overlapping metabolites with faster exchange rates (e.g. amines) is reduced; and (iv) a rapid duty cycle by reducing the SAR is offered resulting in a short scan time which is paramount in acute stroke cases. However, a shortcoming of the lower power pulses is that there is insufficient dynamic range for B_1 correction. B_0 was addressed by centering the voxel-wise z-spectrum, but the B_1 saturation profile, especially at the top and bottom of the imaging slab may show inhomogeneities, such as decreased saturation in the center of the brain. Singh et al (42) demonstrated a method for B_1 correction of CEST spectra optimized for glutamate amine exchange, but a higher power than that chosen in our study would have to be employed for a similar correction. It should not go without notice, however, that B_1 correction (in addition to B_0 correction) should not generally be excluded. Further studies are needed to assess the optimal RF irradiation scheme that can maximize contrast from different tissue types in different stages of stroke evolution. However, our simulations of the pulse sequence parameters show that experimental data and theoretical values are in good agreement and are sensitive to subtle shifts in the exchange rate that may be present in acute stroke, yet slightly increased B_1 (e.g., 1 μT) in potential conjunction with navigator images and multiplex acquisitions may help to reduce the above limitations and reduce scan time.

Limitations

There are several limitations to our study. We were only able to include a limited number of patients due to ethical considerations, as thrombolytic therapy must not be delayed by even a short MRI sequence. This biases the results necessarily because patients with very acute infarctions without any contraindications to intravenous tPA treatment could not be included. MRI-compatible intravenous syringe pumps for tPA would redress this problem and provide opportunities for larger studies. Moreover, our patient population received different treatments, some of them even none, which inevitably results in a tremendously

variable degree of recovery. A conclusion on a group level is therefore not particularly appropriate. We therefore interpret the conclusions conservatively. The complexity of this method with many different factors influencing image contrast and the relatively fast metabolic changes during the course of ischemia makes larger studies necessary. Moreover, about a quarter of patients wake up with stroke symptoms and are currently not eligible for tPA treatment or mechanical thrombectomy (43). Detailed metabolic imaging during infarct progress might help in the future to make treatment available to this large patient group.

In conclusion, we have shown that clinical application of APT imaging in acute stroke patients is possible and carries potential for providing additional information on metabolic changes in acute ischemia not apparent from perfusion- or diffusion-weighted imaging. Quantification of the APT effect can be achieved using both Lorentzian and asymmetry approaches in most patients. We believe that larger scale trials of CEST in human acute stroke patients are warranted and robust, motion-desensitized acquisition and post-processing methods should be developed.

Acknowledgments

Funding: This work was supported in part by the NIH/NINDS (5R01NS078828-02), NIH/NIBIB (5K01EB009120)

This work was supported in part by the NIH/NINDS (5R01NS078828-02).

List of Abbreviations

ADC	apparent diffusion coefficient
APT	amide proton transfer
CEST	chemical exchange saturation transfer
DWI	diffusion weighted imaging
EP	endovascular procedures
FLAIR	FLuid Attenuated Inversion Recovery
MCA	middle cerebral artery
MT	magnetization transfer
NIHSS	National Institutes of Health Stroke Scale
NOE	Nuclear Overhauser Effect
Ppm	points per million
PWI	perfusion weighted imaging
RF	radiofrequency
ROI	region of interest
SNR	signal-to-noise ratio
SPM	Structural Brain Mapping

TFE	turbo field echo
tPA	tissue plasminogen activator
TTP	Time-to-peak

References

1. Hacke W, Kaste M, Bluhmki E, Brozman M, Davalos A, Guidetti D, Larrue V, Lees KR, Medeghri Z, Machnig T, Schneider D, von Kummer R, Wahlgren N, Toni D. Thrombolysis with alteplase 3 to 4. 5 hours after acute ischemic stroke. The New England journal of medicine. 2008; 359(13):1317–1329. [PubMed: 18815396]
2. Wechsler LR. Intravenous thrombolytic therapy for acute ischemic stroke. The New England journal of medicine. 2011; 364(22):2138–2146. [PubMed: 21631326]
3. Hesselmann V, Niederstadt T, Dziewas R, Ritter M, Kemmling A, Maintz D, Koehler M, Seifarth H, Jacobs AH, Ringelstein EB, Heindel W. Reperfusion by combined thrombolysis and mechanical thrombectomy in acute stroke: effect of collateralization, mismatch, and time to and grade of recanalization on clinical and tissue outcome. AJNR Am J Neuroradiol. 2012; 33(2):336–342. [PubMed: 22095969]
4. Broderick JP, Palesch YY, Demchuk AM, Yeatts SD, Khatri P, Hill MD, Jauch EC, Jovin TG, Yan B, Silver FL, von Kummer R, Molina CA, Demaerschalk BM, Budzik R, Clark WM, Zaidat OO, Malisch TW, Goyal M, Schonewille WJ, Mazighi M, Engelter ST, Anderson C, Spilker J, Carrozzella J, Ryckborst KJ, Janis LS, Martin RH, Foster LD, Tomsick TA. Endovascular therapy after intravenous t-PA versus t-PA alone for stroke. The New England journal of medicine. 2013; 368(10):893–903. [PubMed: 23390923]
5. Fiehler J, Foth M, Kucinski T, Knab R, von Bezold M, Weiller C, Zeumer H, Rother J. Severe ADC decreases do not predict irreversible tissue damage in humans. Stroke. 2002; 33(1):79–86. [PubMed: 11779893]
6. Rivers CS, Wardlaw JM. What has diffusion imaging in animals told us about diffusion imaging in patients with ischaemic stroke? Cerebrovasc Dis. 2005; 19(5):328–336. [PubMed: 15795508]
7. Parsons MW, Yang Q, Barber PA, Darby DG, Desmond PM, Gerraty RP, Tress BM, Davis SM. Perfusion magnetic resonance imaging maps in hyperacute stroke: relative cerebral blood flow most accurately identifies tissue destined to infarct. Stroke. 2001; 32(7):1581–1587. [PubMed: 11441205]
8. Kamalian S, Konstas AA, Maas MB, Payabvash S, Pomerantz SR, Schaefer PW, Furie KL, Gonzalez RG, Lev MH. CT perfusion mean transit time maps optimally distinguish benign oligemia from true “at-risk” ischemic penumbra, but thresholds vary by postprocessing technique. AJNR Am J Neuroradiol. 2012; 33(3):545–549. [PubMed: 22194372]
9. Kidwell CS, Alger JR, Saver JL. Evolving paradigms in neuroimaging of the ischemic penumbra. Stroke. 2004; 35(11 Suppl 1):2662–2665. [PubMed: 15472112]
10. Rivers CS, Wardlaw JM, Armitage PA, Bastin ME, Carpenter TK, Cvoro V, Hand PJ, Dennis MS. Do acute diffusion- and perfusion-weighted MRI lesions identify final infarct volume in ischemic stroke? Stroke. 2006; 37(1):98–104. [PubMed: 16322499]
11. Hossmann KA. Cerebral ischemia: models, methods and outcomes. Neuropharmacology. 2008; 55(3):257–270. [PubMed: 18222496]
12. Mori S, Eleff SM, Pilatus U, Mori N, van Zijl PC. Proton NMR spectroscopy of solvent-saturable resonances: a new approach to study pH effects in situ. Magn Reson Med. 1998; 40(1):36–42. [PubMed: 9660550]
13. van Zijl PC, Zhou J, Mori N, Payen JF, Wilson D, Mori S. Mechanism of magnetization transfer during on-resonance water saturation. A new approach to detect mobile proteins, peptides, and lipids. Magn Reson Med. 2003; 49(3):440–449. [PubMed: 12594746]
14. Zhou J, van Zijl PC. Defining an Acidosis-Based Ischemic Penumbra from pH-Weighted MRI. Transl Stroke Res. 2011; 3(1):76–83. [PubMed: 22408691]

15. Sun PZ, Zhou J, Sun W, Huang J, van Zijl PC. Detection of the ischemic penumbra using pH-weighted MRI. J Cereb Blood Flow Metab. 2007; 27(6):1129–1136. [PubMed: 17133226]
16. Sun PZ, Cheung JS, Wang E, Lo EH. Association between pH-weighted endogenous amide proton chemical exchange saturation transfer MRI and tissue lactic acidosis during acute ischemic stroke. J Cereb Blood Flow Metab. 2011; 31(8):1743–1750. [PubMed: 21386856]
17. Broughton BR, Reutens DC, Sobey CG. Apoptotic mechanisms after cerebral ischemia. Stroke. 2009; 40(5):e331–339. [PubMed: 19182083]
18. Kristian T, Siesjo BK. Calcium in ischemic cell death. Stroke. 1998; 29(3):705–718. [PubMed: 9506616]
19. Zaharchuk G, Yamada M, Sasamata M, Jenkins BG, Moskowitz MA, Rosen BR. Is all perfusion-weighted magnetic resonance imaging for stroke equal? The temporal evolution of multiple hemodynamic parameters after focal ischemia in rats correlated with evidence of infarction. J Cereb Blood Flow Metab. 2000; 20(9):1341–1351. [PubMed: 10994856]
20. Orlowski P, Chappell M, Park CS, Grau V, Payne S. Modelling of pH dynamics in brain cells after stroke. Interface Focus. 2011; 1(3):408–416. [PubMed: 22419985]
21. Tee YK, Khrapitchev AA, Sibson NR, Payne SJ, Chappell MA. Evaluating the use of a continuous approximation for model-based quantification of pulsed chemical exchange saturation transfer (CEST). J Magn Reson. 2012; 222:88–95. [PubMed: 22858666]
22. Chappell MA, Donahue MJ, Tee YK, Khrapitchev AA, Sibson NR, Jezzard P, Payne SJ. Quantitative Bayesian model-based analysis of amide proton transfer MRI. Magn Reson Med. 2013; 70(2):556–557. [PubMed: 23008121]
23. Sun PZ. Simplified and scalable numerical solution for describing multi-pool chemical exchange saturation transfer (CEST) MRI contrast. J Magn Reson. 2010; 205(2):235–241. [PubMed: 20570196]
24. Donahue, MJ.; Tietze, A.; Mikkelsen, IK.; Ostergaard, L.; Strother, MK.; Smith, SA.; Blicher, J. Application of Chemical Exchange Saturation Transfer (CEST) MRI in Acute Human Stroke Patients Demonstrates New Potential for Visualization of Tissue Acidosis and Infarction Risk. Salt Lake City, USA: 2013.
25. Ostergaard L, Weisskoff RM, Chesler DA, Gyldensted C, Rosen BR. High resolution measurement of cerebral blood flow using intravascular tracer bolus passages. Part I: Mathematical approach and statistical analysis. Magn Reson Med. 1996; 36(5):715–725. [PubMed: 8916022]
26. Ostergaard L, Sorensen AG, Kwong KK, Weisskoff RM, Gyldensted C, Rosen BR. High resolution measurement of cerebral blood flow using intravascular tracer bolus passages. Part II: Experimental comparison and preliminary results. Magn Reson Med. 1996; 36(5):726–736. [PubMed: 8916023]
27. Ashburner J, Friston KJ. Voxel-based morphometry--the methods. Neuroimage. 2000; 11(6 Pt 1): 805–821. [PubMed: 10860804]
28. Jones CK, Polders D, Hua J, Zhu H, Hoogduin HJ, Zhou J, Luijten P, van Zijl PC. In vivo three-dimensional whole-brain pulsed steady-state chemical exchange saturation transfer at 7 T. Magn Reson Med. 2012; 67(6):1579–1589. [PubMed: 22083645]
29. Mulkern RV, Williams ML. The general solution to the Bloch equation with constant rf and relaxation terms: application to saturation and slice selection. Med Phys. 1993; 20(1):5–13. [PubMed: 8455512]
30. Desmond KL, Stanisz GJ. Understanding quantitative pulsed CEST in the presence of MT. Magn Reson Med. 2012; 67(4):979–990. [PubMed: 21858864]
31. Zhou J, Payen JF, Wilson DA, Traystman RJ, van Zijl PC. Using the amide proton signals of intracellular proteins and peptides to detect pH effects in MRI. Nat Med. 2003; 9(8):1085–1090. [PubMed: 12872167]
32. Zhou J, Wilson DA, Sun PZ, Klaus JA, Van Zijl PC. Quantitative description of proton exchange processes between water and endogenous and exogenous agents for WEX, CEST, and APT experiments. Magn Reson Med. 2004; 51(5):945–952. [PubMed: 15122676]
33. MacMillan EL, Chong DG, Dreher W, Henning A, Boesch C, Kreis R. Magnetization exchange with water and T1 relaxation of the downfield resonances in human brain spectra at 3. 0 T. Magn Reson Med. 2011; 65(5):1239–1246. [PubMed: 21394768]

34. Hua J, Jones CK, Blakeley J, Smith SA, van Zijl PC, Zhou J. Quantitative description of the asymmetry in magnetization transfer effects around the water resonance in the human brain. Magn Reson Med. 2007; 58(4):786–793. [PubMed: 17899597]
35. Yarnykh VL. Pulsed Z-spectroscopic imaging of cross-relaxation parameters in tissues for human MRI: theory and clinical applications. Magn Reson Med. 2002; 47(5):929–939. [PubMed: 11979572]
36. Zu Z, Li K, Janve VA, Does MD, Gochberg DF. Optimizing pulsed-chemical exchange saturation transfer imaging sequences. Magn Reson Med. 2011; 66(4):1100–1108. [PubMed: 21432903]
37. Jones CK, Huang A, Xu J, Edden RA, Schar M, Hua J, Oskolkov N, Zaca D, Zhou J, McMahon MT, Pillai JJ, van Zijl PC. Nuclear Overhauser enhancement (NOE) imaging in the human brain at 7T. Neuroimage. 2013; 77:114–124. [PubMed: 23567889]
38. Zhao X, Wen Z, Huang F, Lu S, Wang X, Hu S, Zu D, Zhou J. Saturation power dependence of amide proton transfer image contrasts in human brain tumors and strokes at 3 T. Magn Reson Med. 2011; 66(4):1033–1041. [PubMed: 21394783]
39. Levine SR, Helpern JA, Welch KM, Vande Linde AM, Sawaya KL, Brown EE, Ramadan NM, Deveshwar RK, Ordidge RJ. Human focal cerebral ischemia: evaluation of brain pH and energy metabolism with P-31 NMR spectroscopy. Radiology. 1992; 185(2):537–544. [PubMed: 1410369]
40. Jokivarsi KT, Grohn HI, Grohn OH, Kauppinen RA. Proton transfer ratio, lactate, and intracellular pH in acute cerebral ischemia. Magn Reson Med. 2007; 57(4):647–653. [PubMed: 17390356]
41. Smith SA, Bulte JW, van Zijl PC. Direct saturation MRI: theory and application to imaging brain iron. Magn Reson Med. 2009; 62(2):384–393. [PubMed: 19526497]
42. Singh A, Cai K, Haris M, Hariharan H, Reddy R. On B1 inhomogeneity correction of in vivo human brain glutamate chemical exchange saturation transfer contrast at 7T. Magn Reson Med. 2013; 69(3):818–824. [PubMed: 22511396]
43. Fink JN, Kumar S, Horkan C, Linfante I, Selim MH, Caplan LR, Schlaug G. The stroke patient who woke up: clinical and radiological features, including diffusion and perfusion MRI. Stroke. 2002; 33(4):988–993. [PubMed: 11935049]

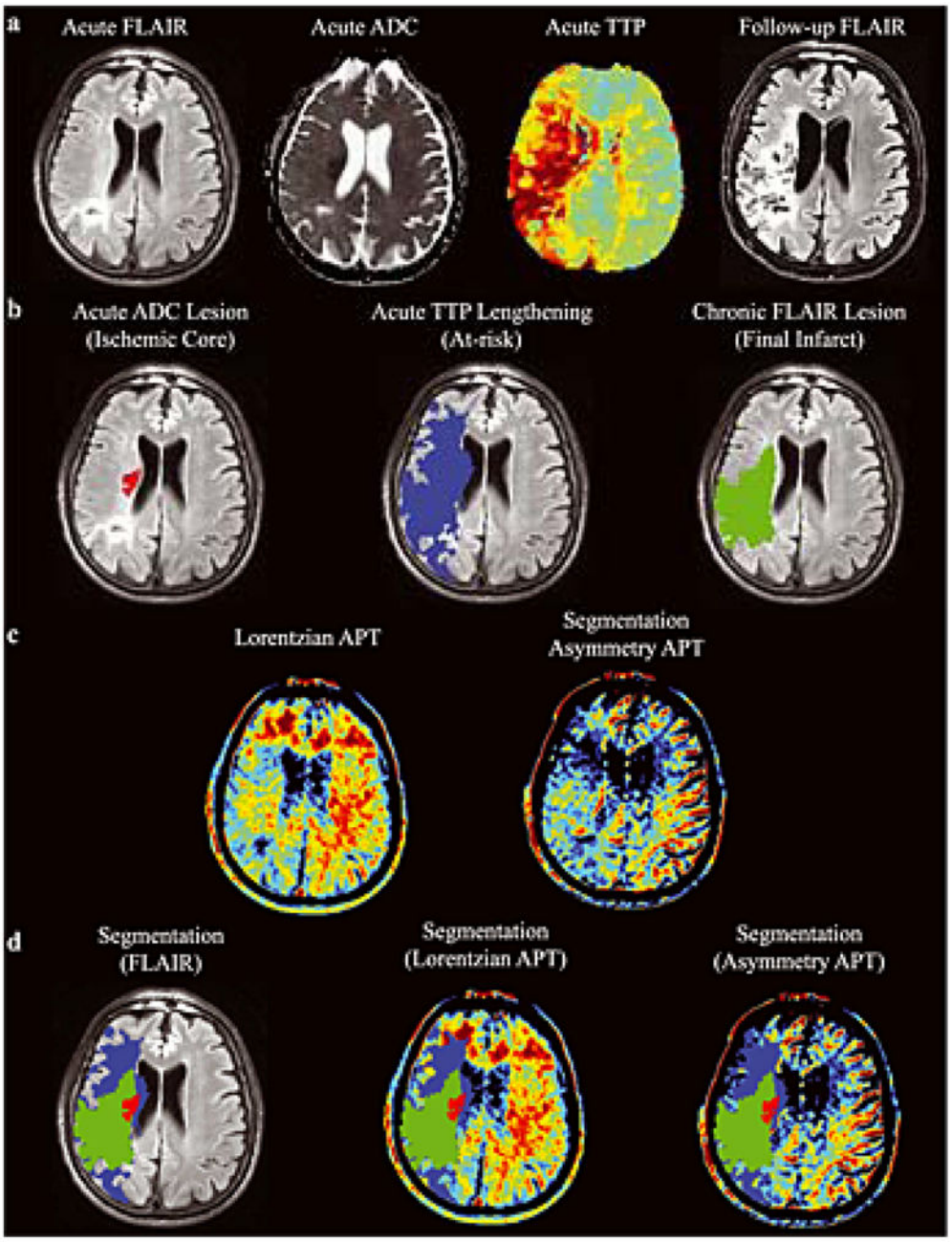

Figure 1. Analysis pipeline

(a) Example of acute T2 FLuid Attenuated Inversion Recovery (T2 FLAIR), apparent diffusion coefficient (ADC), time-to-peak (TTP) and follow-up (>1 month) T2 FLAIR image. (b) Semi-automated segmentation is used to define the ischemic core, which outlines hypointensity in the acute ADC map, the at-risk tissue, defined as lengthening on the TTP map, and the final infarct volume, defined as hyperintensity on the follow-up T2 FLAIR. (c) The APT maps, calculated according to the Lorentzian and asymmetry approaches. (d) Each region is overlaid on the co-registered acute images and the mean intensity is calculated within the separate regions (acute T2 FLAIR and amide proton transfer, APT, maps shown).

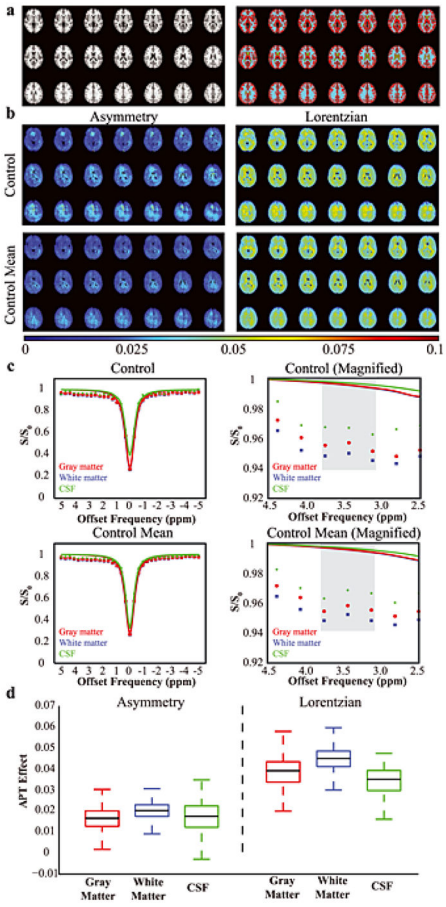

Figure 2. Control volunteer results (n = 5)

(a) To allow for comparison between different tissue types, control data were co-registered to a standard T1-weighted atlas and gray matter (red), white matter (blue) and CSF (green) masks derived from the Harvard-Oxford Cortical Atlas were applied. (b) APT data from a representative control volunteer and from all control volunteers (mean), separately for the asymmetry and Lorentzian analysis approaches. (c) Z-spectra for the representative control volunteer and the mean of all control volunteers. On right, a magnification is show to highlight the small differences in the APT effect at 3.8–3.2 ppm (gray). The colored lines denote the Lorentzian fit to the full z-spectrum. Importantly, note that the Lorentzian fit is predominately sensitive to the data points near the water resonance where the residuals have the potential to be highest and is essentially unity near the amide resonance. (d) A boxplot showing the APT values in the different tissue types. The black line denotes the median, the upper and lower lines denote the upper 75th percentile of the data and lower 25th percentile of the data, and the whiskers extend to the remaining data points.

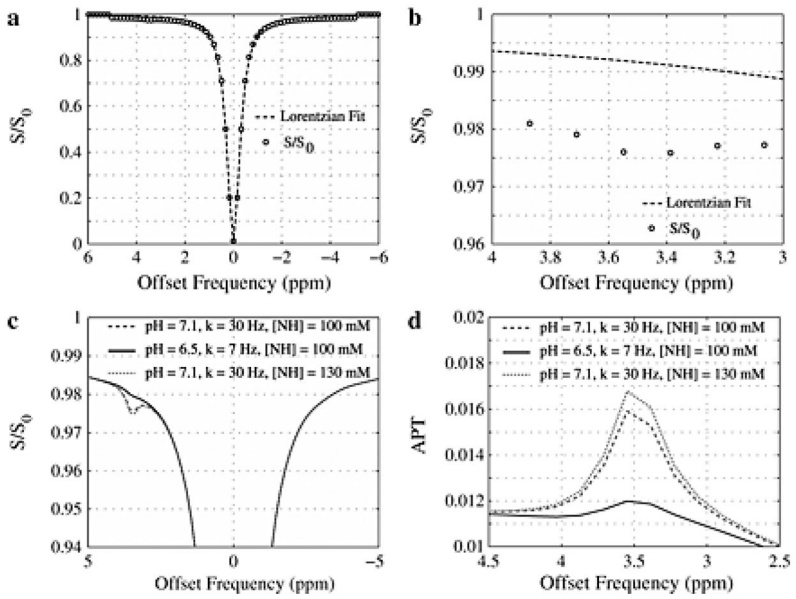

Figure 3. Simulations of expected contrast from the fast, low-power method

(a) The Lorentzian fit and corresponded simulated data shows a small reduction in signal intensity at 3.5 ppm, which is more obvious when (b) the plot is magnified. (c) Differences in the APT effect and (d) difference between the Lorentzian and simulated data for different exchange rates. Importantly, a reduction in pH will reduce the exchange rate and therefore APT effect.

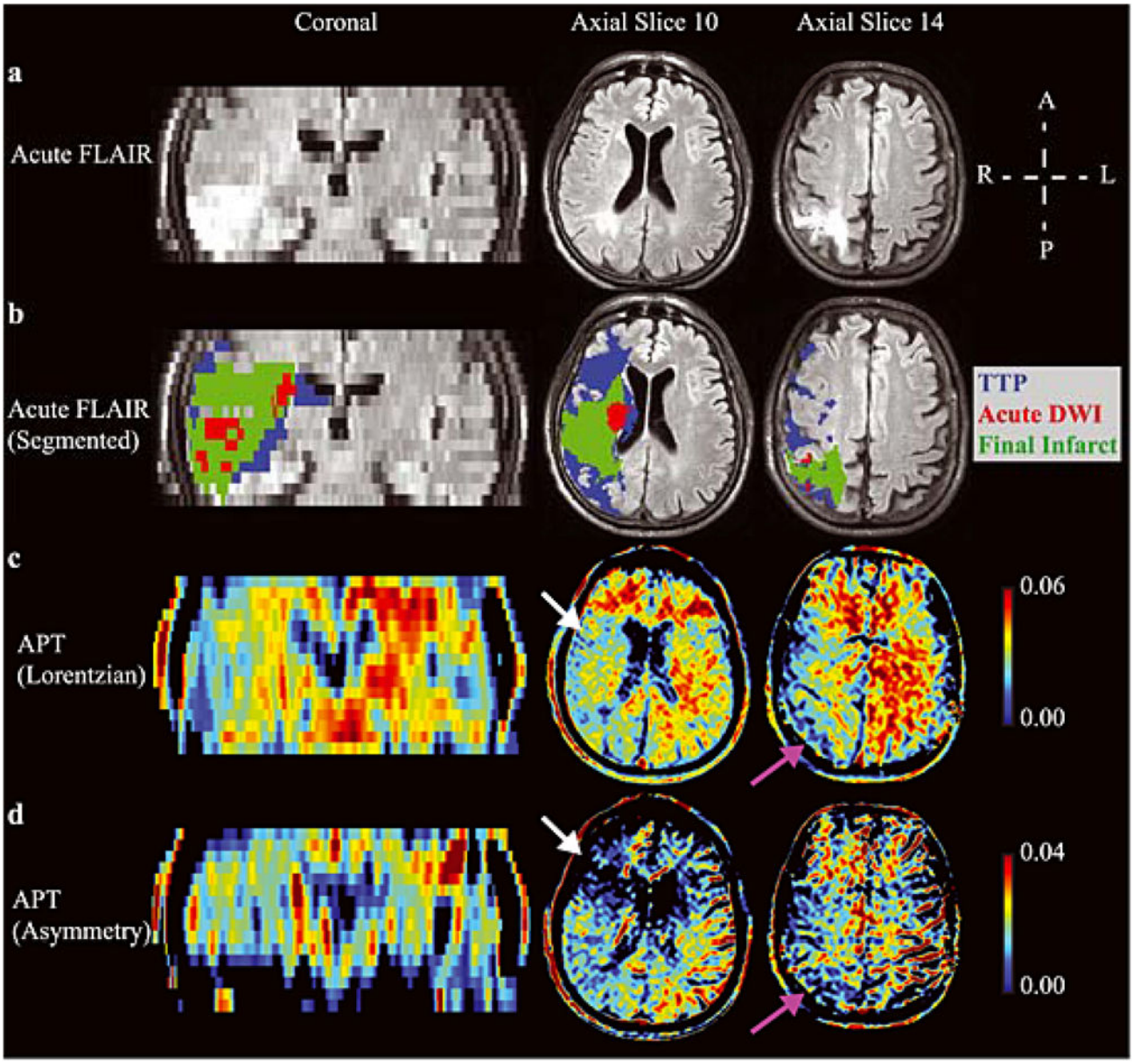

Figure 4. Lorentzian vs. asymmetry analysis

(a) Acute FLuid Attenuated Inversion Recovery (FLAIR) and (b) the segmented regions-of-interest overlaid on the acute FLAIR image in an example patient (Patient 4; Table 1), along with the hyperacute amide proton transfer (APT) maps calculated from the (c) Lorentzian method (d) and asymmetry method. A coronal slice and two axial slices are shown. APT effects are reduced on the acutely ischemic (right) side (white arrows), as well as in regions of prior infarct (purple arrows). The Lorentzian method provides contrast more visually consistent with the pathology than does the asymmetry method, which may be attributed to intra-scan motion across offsets and concomitant MT/NOE/aliphatic contamination of the APT effect. Both methods are compared in Fig. 6.

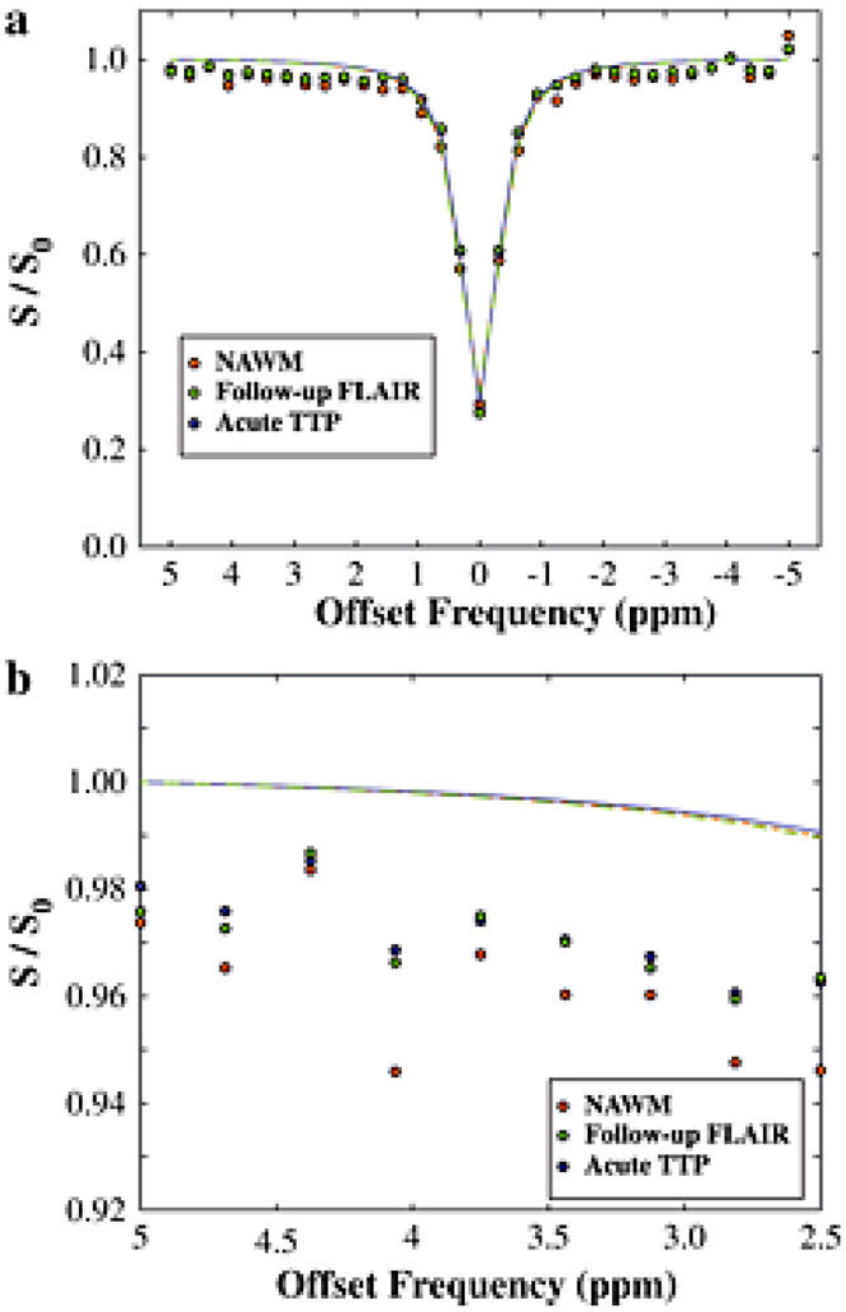

Figure 5. Patient Z-spectrum

(a) The z-spectrum, along with Lorentzian fit, for the patient shown in Fig. 4. (b) Magnification of the z-spectrum in the region of the APT effect shows only a very slightly reduced APT effect in the region progressing to infarction and in the time-to-peak (TTP) lengthening region relative to normal-appearing-white-matter (NAWM). These very small effects are largely consistent in magnitude with simulation expectations (Fig. 3).

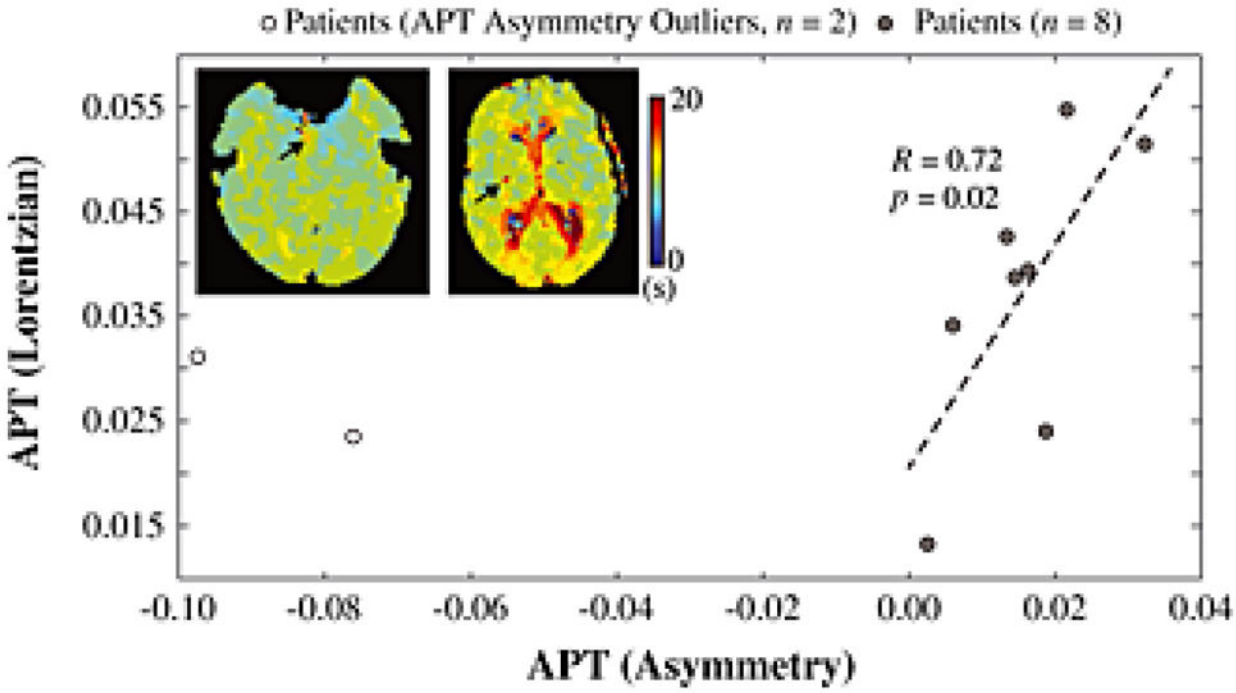

Figure 6. Comparison of APT analysis approaches

In 8/10 patients, the Lorentzian APT analysis was tightly correlated with the asymmetry analysis (R=0.72; P=0.02). However, in two patients the APT asymmetry analysis provided negative values that met outlier criteria (white circles; representative time-to-peak, TTP, maps shown with arrows pointing to TTP lengthened regions). As can be seen, these two patients had very small ischemic regions, suggesting the asymmetry analysis may be less reliable when considering very small regions-of-interest, likely owing to reduced SNR secondary to propagation of error arising from comparison of two data points acquired at different times.

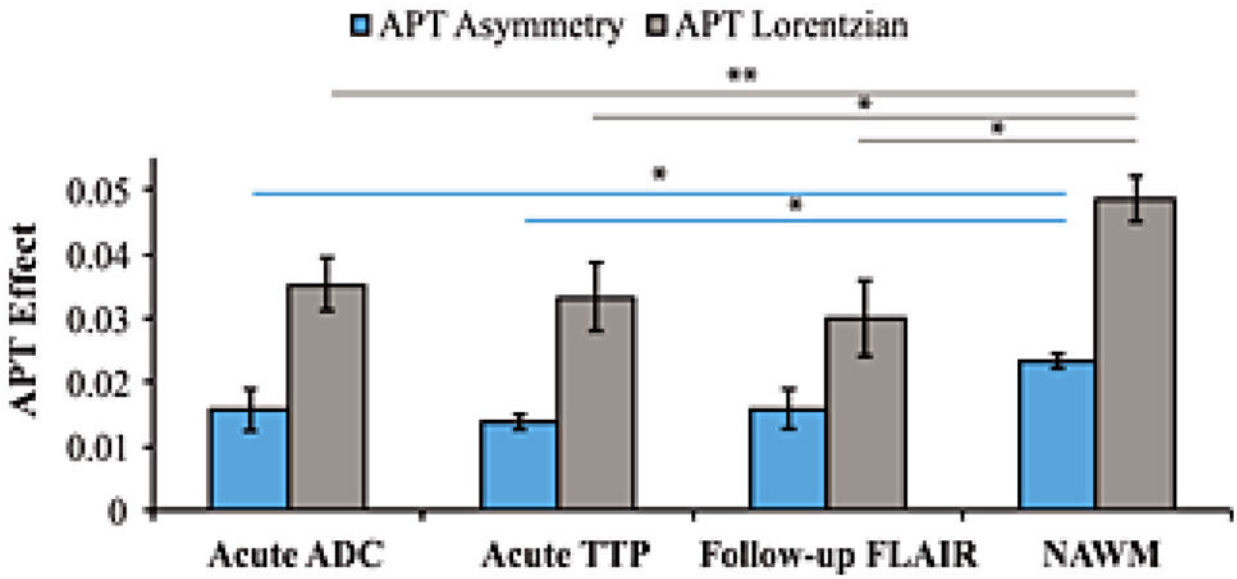

Figure 7. Group results

Bar graph showing the amide proton transfer (APT) effect (separately for the asymmetry and Lorentzian approaches) for all patients in different segmented regions-of-interst. The two patients with negative asymmetry (Fig. 6) were excluded in the asymmetry analysis. In both analyses, normal appearing white matter (NAWM) gave larger APT effects than different ischemic regions (P=0.03), however no significant finding was observed between the size of the APT effect within the different ischemic regions. Error bars denote standard error. * P<0.05. **P≤0.01.

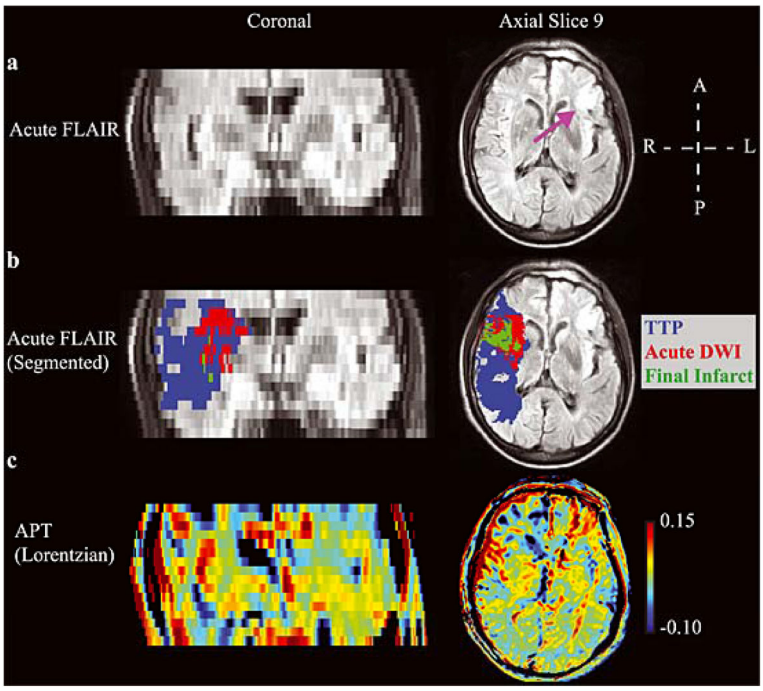

Figure 8. Example patient highlighting the multiple difficulties of performing APT imaging in human acute stroke patients

(a) The acute FLuid Attenuated Inversion Recovery (FLAIR) image denotes clear motion artifacts, which were observed in the majority of patients, as well as a right-sided prior infarct (purple arrow). (b) The segmentation results showing a large ischemic penumbra. In this patient, the region of diffusion weighted imaging (DWI) contrast largely co-localized with the final infarct volume (green). (c) The APT map shows less asymmetry than apparent in the patient presented in Fig. 4, which is partly consistent with more limited tissue acidosis. However, high APT values are observed in the sulcus on the right, which partial volumes with CSF. Additionally, regions of the right frontal lobe exhibit apparent reduced APT effects, yet these regions do not progress to infarct and in some instances appear to partial volume with the chronic infarct. Improved approaches for correcting motion and partial volume effects are likely required before more widespread testing of APT is pursued in acute stroke patients.

Table 1

Clinical details of all patients

NIHSS: National Institute of Health Stroke Scale. Note: all values are calculated from the hyperacute scans with the different masks calculated from the multimodal data (Fig. 1).

Patient ID	Age (yrs)/Sex	NIHSS at arrival	Time since symptom onset	Treatment	Stroke location	Symptoms	Time (days) until follow-up MRI
1	57/M	15	1h 10 min	i.v. thrombolysis and thrombectomy	Right M1 Occlusion	Left-sided hempiaresis	32
2	62/F	2	1h 32 min	none	Occlusion of one of the deep penetrating arteries arising from right M1	Left-sided hemiparesis	33
3	89/F	8	2h 25 min	iv thrombolysis	Occlusion of cerebelli superior artery branches	Left hemiparesis and dysarthria	Not performed
4	58/M	16	1–4h	thrombectomy	Right M1 Occlusion	Paralysis of left arm and left; left-sided hypaesthesia	92
5	72/F	2	1h 5 min	none	Occlusion of one of the deep penetrating arteries arising from M1 and occlusion in posterior watershed	Right-sided hemiparesis	47
6	69/M	15	1–7h	none	Right M1 Occlusion and left posterior watershed	Left-sided hemiparalysis, left-sided facial nerve paresis, neglect	Not performed
7	72/M	17	1h 20 min	none	Left M2 Occlusion	Aphasia and right-sided paresis	23
8	73/M	0	1h 15 min	none	Occlusion of branches of basilar artery	Short-term left-sided hemiparalysis and syncope prior to arrival	41
9	74/M	6	< 24hr	none	Right M2 Occlusion	Left-sided arm paresis	47
10	68/M	3	< 24hr	none	Occlusion of one of the deep penetraring arteries arising from right M1	Left-sided hemiparesis, and facial nerve paresis; dizziness	42

Table 2

Imaging findings from all patients

No difference in the apparent diffusion coefficient (ADC) between the time-to-peak (TTP) region and penumbra tissue was noted (P = 0.25), whereas significantly lower ADC was measured in both the ischemic core and tissue progressing to infarction (P < 0.001). There was no significant difference of the TTP or the T2 FLuid Attenuated Inversion Recovery (T2 FLAIR) data between any of the four regions. Finally, a trend for a mean reduction in amide proton transfer (APT) was found between the at-risk tissue and final infarct volume (P = 0.10), and all ischemic regions had lower APT effects relative to normal-appearing-white-matter (NAWM).

	Volume (mL)			ADC (a.u.)				TTP (s)				APT (Lorentzian)			
Patient ID	**Core**	**TTP Lengthening**	**Final Infarct**	**Core**	**TTP Lengthening**	**Final Infarct**	**NAWM**	**Core**	**TTP Lengthening**	**Final Infarct**	**NAWM**	**Core**	**TTP Lengthening**	**Final Infarct**	**NAWM**
1	34.3	174.5	11.2	506	952	222	771	28.9	23.9	35.8	10.7	0.038	0.022	0.020	0.056
2	0.5	0.0	0.4	511	NA	278	764	8.8	NA	8.6	8.9	0.013	NA	0.008	0.028
3	6.8	35.9	NA	441	959	NA	782	27.4	28.5	NA	22.7	0.054	0.059	NA	0.052
4	5.2	194.4	138.7	444	1132	981	754	19.2	15.7	15.9	8.3	0.034	0.030	0.033	0.039
5	0.6	0.0	1.2	549	NA	705	833	7.7	NA	8.0	6.0	0.052	NA	0.056	0.049
6	51.3	186.0	NA	576	1136	NA	864	30.6	23.4	NA	9.9	0.043	0.033	NA	0.062
7	3.3	19.5	1.7	518	1171	1038	761	15.2	22.9	25.9	14.9	0.039	0.045	0.043	0.048
8	0.6	0.2	0.0	542	563	NA	782	11.7	13.1	NA	9.6	0.031	0.010	NA	0.056
9	7.3	18.6	4.8	511	1013	745	795	13.6	23.0	14.3	11.7	0.024	0.029	0.024	0.037
10	0.947	0.183	1.663	348.07	523.6	449.8	770.8	12.86	14.58	12.67	11.32	0.023	0.039	0.026	0.059